Chamber And Orifice-Plate Attenuators For Rectangular Tunnel Blast Pressure

Cheng-Wei Hung[1] and Pen-Chou Chen[2*]

[1] Department of Civil Engineering and Environmental Informatics, Minghsin University of Science and Technology, Hsinchu 30401, Taiwan
[2] Department of Civil Engineering, National Chung Hsing University, Taichung 40227, Taiwan
[*] Corresponding author. E-mail: s883309kimo@gmail.com

Received: May. 06, 2026; Accepted: Jun. 19, 2026

External explosions near tunnel entrances can transmit severe shock waves into rectangular underground passages. This study experimentally compares three compact internal blast-pressure reduction configurations: an expansion chamber, a single-orifice plate, and a double-orifice plate. Scaled C4 explosive tests were conducted using 100-350g charges located 60 cm from the tunnel entrance and aligned with the tunnel centreline. A rectangular steel tunnel model with a 30 cm $\times$ 30 cm internal cross-section and a total length of 200 cm was instrumented at $L/D = 0.07$, 1.00, 3.00, and 5.67. The main attenuation index was the downstream-to-upstream peak-pressure ratio between $L/D = 3.00$ and $L/D = 5.67$. Across the five charge masses, the expansion chamber, single-orifice plate, and double-orifice plate produced mean experimental pressure reductions of $29.9 \pm 9.9\%$, $51.2 \pm 6.1\%$, and $81.9 \pm 3.8\%$, respectively. The double-orifice configuration provided the strongest attenuation because it introduced two sequential restriction and diffraction stages. For the expansion chamber, the downstream pressure represents an intra-chamber measurement and should not be interpreted as a post-chamber transmission coefficient. The numerical observations are retained only as supplementary qualitative interpretation; the experimental results form the quantitative basis of the conclusions. The findings provide a bounded experimental ranking of compact geometric attenuation devices for rectangular tunnel blast mitigation, rather than a general design standard.

Keywords: confined blast; pressure reduction; scaled explosive testing; geometric restriction; shock-wave diffraction; protective design

http://dx.doi.org/10.6180/jase.202611_34.002

1. Introduction

Underground facilities, tunnel entrances, ventilation ducts, and access passages are vulnerable to external explosions because shock waves can enter confined passages and propagate over considerable distances [1–6]. Once the blast wave is transmitted into a passage, wall confinement, repeated reflection, diffraction, and local geometric discontinuities may alter the internal pressure field[1, 4, 6]. This study considers rectangular utility or protective tunnel passages as the representative scenario. Protective design therefore requires not only portal-pressure estimation but also internal mitigation strategies capable of reducing pressure transmission downstream of critical entrances or ventilation paths[7, 8].

Recent research has shown that blast-wave interaction with internal obstacles or geometric discontinuities can significantly alter downstream loading. Barrier-type devices, branching layouts, and porous or perforated components can reduce the transmitted wave by forcing reflection, diffraction, separation, and redistribution [9–

12]. The single- and double-barrier studies by Berger et al. [13, 14] are especially relevant because they demonstrate that attenuation is governed by geometric blockage and repeated diffraction; however, those studies focused on barrier-type configurations rather than comparing a volume-enlargement chamber with one- and two-stage orifice-plate attenuators in the same rectangular tunnel system. Accordingly, fewer studies provide a consistent experimental comparison between expansion-type and orifice-type attenuation devices within the same rectangular tunnel configuration.

Expansion chambers and orifice plates represent two practical but physically distinct mitigation concepts. An expansion chamber increases the local flow volume and cross-sectional area, encouraging wave expansion and partial energy redistribution [15]. An orifice plate reduces the available flow area, producing upstream reflection and downstream diffraction through the opening [9]. A double-orifice arrangement may further improve attenuation through repeated restriction and diffraction [10, 14]. The opening ratio is particularly important because it controls the fraction of the tunnel area available for shock transmission and has been identified in the barrier literature as a dominant geometric parameter for attenuation [9, 10, 12, 13].

The objective of this study is to compare the blast-pressure reduction performance of an expansion chamber, a single-orifice plate, and a double-orifice plate installed inside a rectangular steel tunnel model. The study intentionally focuses on internal attenuation-device performance, rather than blast-wall stand-off distance or portal-overpressure prediction. The main contributions are: (1) a consistent scaled experimental comparison of three attenuation configurations; (2) statistical reporting of pressure ratios across five C 4 charge masses; (3) a clarified description of geometry, instrumentation, and evaluation positions; (4) a design-oriented discussion of the 12.6% orifice opening ratio; and (5) a limited, supplementary use of ALE numerical results to support physical interpretation without relying on unvalidated simulations as the primary evidence [16].

2. Materials and methods

2.1. Rectangular tunnel model and scale interpretation

The experimental program used a scaled steel tunnel model with an internal cross-section of 30 cm $\times$ 30 cm, a total length of 200 cm , and a wall thickness of 0.5 cm . The model was assembled from modular components, including 30 cm $\times$ 30 cm $\times$ 60 cm tunnel modules, a 60 cm $\times$ 60 cm $\times$ 60 cm expansion-chamber module, and 30 cm $\times$ 30 cm $\times$ 20 cm orifice-plate modules. The total specimen weight was approximately 200 kg . Steel plates were also placed around the tunnel entrance to ensure that the external blast wave entered the tunnel opening effectively and to reduce undesirable side diffraction near the portal.

The model should be interpreted as a controlled reduced-scale experimental system rather than a direct one-to-one prototype replica. No single full-scale prototype was specified; therefore, the experiments are not presented as a strict geometric scale model such as 1 : 5 or 1 : 10. Instead, this study reports nondimensional positions using L/D, where L is the distance from the tunnel entrance and D = 30 cm is the characteristic tunnel dimension, and compares device performance under identical charge-distance and tunnel-geometry conditions. The results should therefore be used for comparative attenuation assessment within the tested range rather than direct full-scale extrapolation. Where design extrapolation is required, Hopkinson-Cranz similarity and additional full-scale validation should be applied in accordance with established protective-design practice [7, 8].

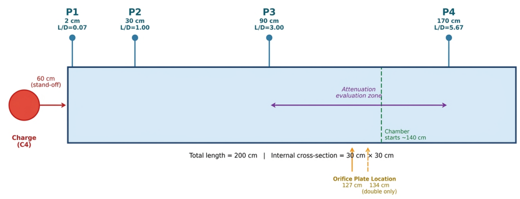

Fig. 1. Experimental layout and pressure-measurement locations

2.2. Attenuation configurations

Four configurations were considered. The baseline rectangular tunnel had no internal attenuation device and was used only as the reference condition. The expansion chamber configuration connected a 30 cm $\times$ 30 cm tunnel to a 60 cm $\times$ 60 cm $\times$ 60 cm chamber, corresponding to a local cross-sectional area ratio of 4.0 relative to the baseline tunnel. Based on the L/D positions used in the attenuation analysis, the chamber was arranged so that the upstream sensor at L/D = 3.00 was approximately 1.67 D before the chamber entrance and the P 4 sensor at L/D = 5.67 was approximately 1.0D inside the enlarged chamber volume.

The single-orifice plate configuration used one circular opening with a diameter of 12 cm . The plate was installed 127 cm from the tunnel entrance. The double-orifice plate configuration used two such plates installed at 127 cm and 134 cm from the tunnel entrance; the centre-to-centre spacing between the two plates was therefore 7 cm (approximately 0.23D). This short spacing was selected as a compact two-stage restriction layout that could be installed within the modular 20 cm plate section, rather than as an optimized spacing for fully redeveloped inter-plate flow.

The tunnel cross-sectional area was 900 cm^2 and the circular orifice area was 113.1 cm^2, giving an opening area ratio of 12.6%. This ratio was selected as a severe but constructible compact-restriction case for comparing single-stage and two-stage attenuation. It is below the opening ratios commonly examined in rigid-barrier attenuation studies, where reducing the opening ratio markedly increases attenuation, and was adopted to test a high-blockage configuration suitable for compact protective layouts. Because only one opening ratio and one double-plate spacing were tested, the results should be interpreted as a device-comparison study rather than a complete opening-ratio or spacing optimization.

This distinction is important for interpretation: in the expansion-chamber case, the downstream evaluation point is located within the chamber itself, while in the orifice-plate cases the downstream evaluation point is located in a downstream tunnel segment after the restriction. The expansion-chamber result is therefore reported as an intra-chamber pressure-reduction measure rather than a post-chamber transmission coefficient.

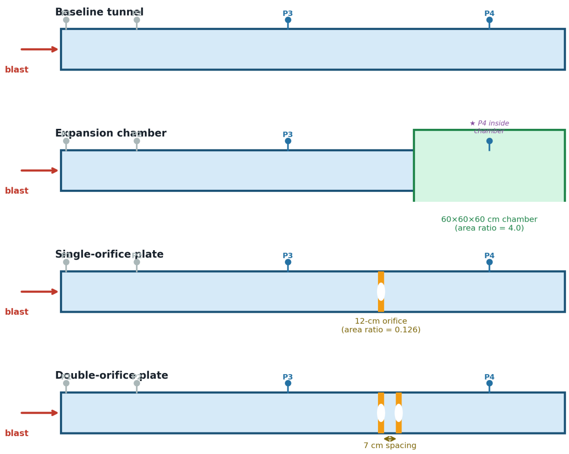

Fig. 2. Tested attenuation configurations: baseline tunnel, expansion chamber, single-orifice plate, and double-orifice plate

2.3. Explosive loading, instrumentation, and measurement positions

C4 explosive charges of 100, 150, 200, 250, and 350 g were used. The charge centre was positioned 60 cm outside the tunnel entrance and 30 cm above the ground, aligned with the tunnel centreline. The explosive was initiated using an M6 electric detonator. The 60 cm external detonation distance was kept constant for all attenuation configurations so that the comparison focused on the internal device geometry rather than loading variation.

Internal pressures were measured at 2, 30, 90, and 170 cm from the tunnel entrance, corresponding to $L/D = 0.07, 1.00, 3.00$, and 5.67. The pressure transducers installed inside the tunnel were PCB 113A23 sensors with a maximum pressure capacity of 103 MPa . According to the manufacturer specification for the 113A23 class sensor, the sensitivity is approximately 0.073mV/kPa, the resolution is on the order of 1.38 kPa for the 113 A 23 specification, and the rise time is less than 1 microsecond [17]. Although the measured peak pressures in this study are much lower than the maximum pressure capacity, they remain well above the sensor resolution and are therefore suitable for dynamic pressure-history comparison. The high range was selected to avoid saturation during near-portal and reflected-pressure events. The transducers were installed in END-ON orientation through the tunnel wall; because the source is an archived experimental dataset, small local installation offsets or minor sensor protrusion relative to the inner wall cannot be completely reconstructed and are treated as potential local measurement uncertainties in the discussion.

The attenuation analysis in this paper uses the pressure at $L/D = 3.00$ as the upstream or predevice value Pu and the pressure at $L/D = 5.67$ as the downstream or device-influenced value Pd . For the orifice-plate configurations, P4 is located in the reduced downstream tunnel section after the plate or plates. For the expansion-chamber configuration, however, P4 is located inside the enlarged chamber volume, not downstream of a chamber exit. Therefore, the expansion-chamber Pd represents an intra-chamber peak pressure under chamber reflection and recompression effects, whereas the orifice-plate Pd represents pressure in a downstream tunnel segment. This methodological difference is explicitly considered in the interpretation and limitations.

2.4. Evaluation indices and statistical treatment

The normalized downstream pressure ratio Rp and pressure-reduction efficiency eta are defined as follows:

$$\mathrm{Rp} = \mathrm{Pd}/\mathrm{Pu} \tag{1}$$

$$\eta = \left(1 - \frac{P_d}{P_u}\right) \times 100\% \tag{2}$$

where Rp is the normalized pressure ratio, eta is the pressure-reduction efficiency, and Pu is the peak overpres-

Table 1. Geometry and design parameters of the tested configurations

Configuration	Primary geometry	Device location / feature	Area or opening ratio	Purpose	P4 sensor relative position
Baseline tunnel	30 × 30 × 200 cm	No internal attenuator	900/900 = 1.00	Reference condition	P4 in straight tunnel at L/D = 5.67
Expansion chamber	60 × 60 × 60 cm chamber	Chamber begins ∼ 140 cm from entrance; P4 located about 1.0D inside the chamber	3600/900 = 4.00	Intra-chamber wave expansion and redistribution	P4 approximately 1.0D inside enlarged chamber
Single-orifice plate	12 cm circular opening	Plate at 127 cm; P3 is 1.23D upstream and P4 is 1.43D downstream	113.1/900 = 0.126	Single-stage restriction and diffraction	P4 approximately 1.43D downstream of the plate
Double-orifice plate	Two 12 cm circular openings	Plates at 127 and 134 cm with 7 cm spacing; P4 is 1.20D downstream of the second plate	113.1/900 = 0.126 per plate	Two-stage restriction and repeated diffraction	P4 approximately 1.20D downstream of the second plate

Table 2. Experimental loading, instrumentation, and measurement definition

Parameter	Value / Range	Role in This Paper
Charge type	C4 explosive	External blast loading
Charge masses	100, 150, 200, 250, and 350 g	Loading variation
External detonation distance	60 cm from tunnel entrance; charge centre 30 cm above ground	Controlled boundary condition
Tunnel dimensions	30 × 30 × 200 cm; wall thickness = 0.5 cm	Scaled rectangular tunnel model
Internal sensors	PCB 113A23; maximum pressure = 103 MPa; END-ON measurement	Internal transmitted pressure
Free-field/reference sensors	PCB 137A23; maximum pressure = 345 kPa; END-ON measurement	Reference measurements in the broader test program
Data acquisition	Agilent 5000-series oscilloscope; 100 MHz bandwidth; maximum 2×10^9 samples/s	Pressure–time recording
Internal measurement points	$L/D = 0.07, 1.00, 3.00, 5.67$	Transmission and attenuation evaluation
Upstream/downstream definition	P_u at $L/D = 3.00$; P_d at $L/D = 5.67$	Pressure-reduction index

sure at L/D = 3.00 and Pd is the peak overpressure at L/D = 5.67. A lower Rp and a higher eta indicate stronger attenuation. Each device was tested under five C 4 charge masses. For each configuration, this paper reports the mean and standard deviation of the pressure-reduction efficiency across the five charge conditions. The n values in Table 3 are the effective pressure records retained in the archived compiled dataset for each charge and measurement location; they differ among charge cases because the original compilation retained valid usable traces rather than a uniform designed repeat count for every cell. Where available from the original experimental records, the number of effective pressure records and the standard deviation of the measured peak pressure at each measurement location are reported. For the single-orifice upstream values, the original compiled attenuation table provides the averaged Pu values used for the reduction calculation under the same boundary conditions, whereas the repeat-test statistics were not available in the same compiled table; these upstream reference values are treated as representative for comparative purposes and are not reconstructed.

Because the five charge cases represent different loading conditions rather than repeated shots at one identical charge mass, the reported standard deviations are interpreted as charge-level variability, not shot-to-shot repeatability. Approximate 95% charge-level confidence intervals for the mean pressure-reduction efficiency are 29.9% ± 12.3% for the expansion chamber, 51.2% ± 7.6% for the single-orifice plate, and 81.9% ± 4.7% for the double-orifice plate. A charge-level paired comparison between the single- and double-orifice configurations showed that the doubleorifice plate reduced the normalized downstream pressure ratio by an additional 0.306 on average; the paired t-test gave $t(4) = 10.98, p = 0.00039$, with a 95% confidence interval of 0.229-0.383 for the additional reduction in Rp. This test is reported only as a trend-supporting check across charge masses and is not presented as shot-to-shot repeatability evidence.

2.5. Supplementary numerical modelling approach

The numerical results are retained only as supplementary interpretation and limited attenuation-ratio checking. The quantitative conclusions of this paper are based on the experimental data. This revision avoids using the ALE simulation as the primary evidence for the device ranking and does not claim a stand-alone computational design method; the modelling is used in the same limited interpretive sense as prior tunnel-pressure attenuation studies [16].

The archived simulations used an Arbitrary Lagrangian-Eulerian framework [18, 19]. The explosive and air domains were modelled using Eulerian solid elements, while the tunnel walls and attenuation devices were represented using structural elements. The explosive was represented using a high-explosive burn material model coupled with a Jones-Wilkins-Lee equation of state. Air was represented using a null material model with a linear polynomial equation of state. The tunnel-domain modelling used local refinement near the charge, portal, gauge locations, and chamber/orifice discontinuities, with coarser cells outside the pressure-extraction and far-tunnel regions. The local free-field mesh class for the $0.10 - 0.35$ kg experimental charge range was approximately $0.031 - 0.046$ cm, based on the archived convergence relationship, and mapping/refinement was used to keep the tunnel-domain model computationally feasible. The outer air-domain limits were treated as open or non-reflecting boundaries in the modelling workflow so that artificial reflection from far-field boundaries would not dominate the extracted tunnel pressures.

The numerical attenuation ratios are compared with the experimental ratios only at the level of normalized downstream peak pressure. The numerical downstream-to-upstream ratio for the single-orifice configuration is consistent with the experimental mean, offering a partial check at the peak-pressure-ratio level. By contrast, the expansion-chamber numerical result overestimates attenuation, so it is used only to discuss mechanism sensitivity rather than to support a quantitative conclusion. The representative archived pressure-time histories in Fig. 4 are adapted from the source thesis numerical results for the tunnel 3 (single-orifice) and tunnel 4 (double-orifice) configurations [20]. They are used only to illustrate waveform shape, arrival sequence, and post-restriction attenuation. Complete experimental pressure-time-history validation, impulse extraction, and independent mesh sensitivity for every device configuration remain outside the scope of this experimental comparison paper.

3. Results and discussion

3.1. Experimental attenuation ratios and statistical summary

Table 3 reports the experimental peak pressures at $L/D = 3.00$ and $L/D = 5.67$, the downstream-to-upstream pressure ratios, and the resulting reduction efficiencies. The statistics demonstrate that the expansion chamber provides moderate attenuation, the single-orifice plate provides stronger attenuation, and the double-orifice plate provides the strongest reduction among the tested configurations.

Note. For the single-orifice configuration, Pu values are compiled upstream reference averages used in the original attenuation calculation under identical boundary conditions; the corresponding repeat-test count and standard deviation were not retained in the same compiled table and are therefore not reconstructed. The n values shown for other cells represent effective pressure records retained in the archived compiled dataset, not a uniform designed repeat count.

To directly address the baseline-reference issue, Table 4 compares the straight baseline tunnel transmission ratio with the three attenuation configurations for each charge mass. This comparison separates the within-device P3-P4 index from the improvement relative to a no-device tunnel.

Relative to the baseline straight tunnel, the mean P4/P3 ratio decreased from 0.86 to 0.70 for the expansion chamber, 0.49 for the single-orifice plate, and 0.18 for the double-orifice plate. The double-orifice configuration had the lowest ratio for every tested charge mass. However, this ranking remains measurement-definition dependent because the expansion-chamber P4 value is an intra-chamber pressure, whereas the orifice-plate P 4 values are downstream tunnel pressures.

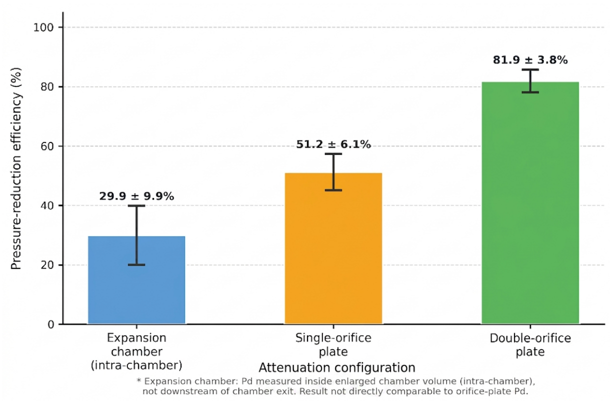

Fig. 3. Experimental pressure-reduction efficiencies; bars show mean values across five charge masses and error bars show standard deviation

In response to the reviewer request for waveform information, the revised manuscript now incorporates the archived numerical pressure-time histories available in the source thesis for the single-orifice and double-orifice configurations. The thesis contains pressure-time history plots for tunnel type 3 and tunnel type 4, corresponding to Fig. 4-29 and Fig. 4-33 in the source document [20]. These histories are not used to calculate the experimental attenu-

Table 3. Experimental peak pressure, downstream pressure ratio, and pressure-reduction efficiency.

Configuration	Charge (g)	P_u (kPa)	n	SD	P_d (kPa)	n	SD	P_d/P_u	Reduction (%)
Expansion chamber	100	282.81	4	51.43	189.52	4	20.98	0.67	33.0
	150	417.29	6	46.76	237.99	6	17.79	0.57	43.0
	200	427.71	7	32.21	332.31	7	19.52	0.78	22.3
	250	468.46	6	65.13	384.24	6	30.28	0.82	18.0
	350	664.85	5	70.65	443.45	5	46.99	0.67	33.3
Mean ± SD								0.70 ± 0.10	29.9 ± 9.9
Single-orifice plate	100	300.49	—	—	123.89	5	7.84	0.41	58.8
	150	367.77	—	—	170.62	5	19.68	0.46	53.6
	200	454.65	—	—	242.00	6	31.28	0.53	46.8
	250	482.50	—	—	272.76	7	36.59	0.57	43.5
	350	747.77	—	—	348.09	10	61.14	0.47	53.4
Mean ± SD								0.49 ± 0.06	51.2 ± 6.1
Double-orifice plate	100	272.79	4	41.03	38.18	4	3.86	0.14	86.0
	150	306.57	4	30.39	52.33	4	7.78	0.17	82.9
	200	450.01	10	76.97	71.64	10	12.69	0.16	84.1
	250	544.88	8	86.76	108.96	8	18.46	0.20	80.0
	350	703.04	5	83.04	166.30	5	18.54	0.24	76.3
Mean ± SD								0.18 ± 0.04	81.9 ± 3.8

Table 4. Charge-wise comparison of baseline and attenuation P4/P3 ratios

Charge (g)	Baseline tunnel P4/P3	Expansion chamber P4/P3	Single-orifice P4/P3	Double-orifice P4/P3
100	0.815	0.67	0.41	0.14
150	0.916	0.57	0.46	0.17
200	0.879	0.78	0.53	0.16
250	0.899	0.82	0.57	0.20
350	0.806	0.67	0.47	0.24
Mean +/- SD	0.86 +/- 0.05	0.70 +/- 0.10	0.49 +/- 0.06	0.18 +/- 0.04

ation ratios; they are included only to show arrival sequence, reflected-wave interaction, post-restriction peak change, and waveform-duration modification. The available source record for the expansion chamber configuration is a pressure-transmission curve rather than a complete pressure-time trace; therefore, the expansion-chamber waveform is not quantified beyond the measured peakpressure ratios.

Fig. 4 Supplementary archived numerical pressure-time histories for the single-orifice and double-orifice configurations, adapted from the source thesis figures for tunnel type 3 and tunnel type 4 [20]. These histories illustrate waveform shape, arrival sequence, and post-restriction attenuation, but they do not replace experimental pressure-time validation.

The representative histories indicate that the orifice restrictions modify not only peak pressure but also arrival sequence and waveform shape. In the single-orifice case, the post-restriction histories show delayed arrivals and a longer decaying pressure train downstream of the plate. In the double-orifice case, the closely spaced plates further alter the downstream wave sequence and create a stronger post-restriction reduction in the archived numerical histories. These observations are used only to support the qualitative mechanism discussion; they are not treated as

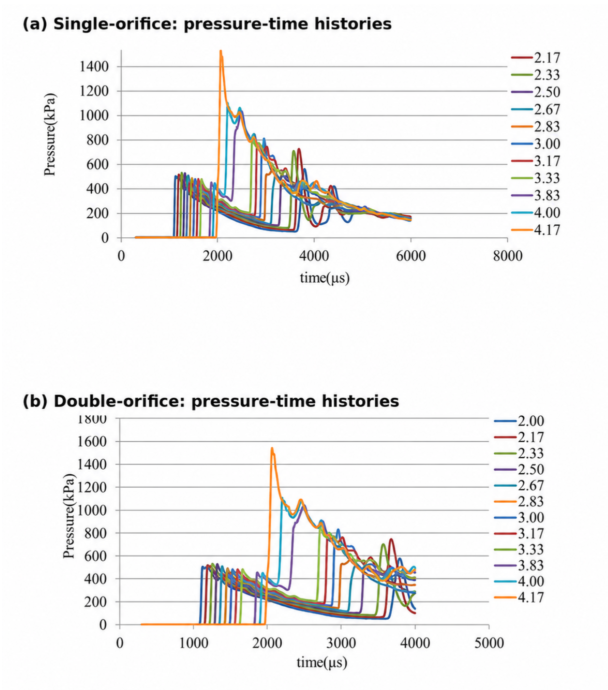

Fig. 4. Supplementary numerical pressure–time histories for the single-orifice and double-orifice tunnel configurations, adapted from the archived figures in the source thesis (Tunnel Types 3 and 4).

independent quantitative evidence for impulse, positive-phase duration, or design-level validation.

3.2. Expansion chamber performance

The expansion chamber reduced the P4 peak pressure by 29.9 ± 9.9% across the five charge masses. Its reduction mechanism is associated with sudden volume enlargement and wave expansion. However, unlike the orifice-plate cases, the P 4 sensor for this configuration was located inside the enlarged chamber volume rather than in a downstream tunnel segment after a chamber exit. The reported 29.9% reduction therefore reflects an intra-chamber pressure level relative to the upstream tunnel pressure at L/D = 3.00, not a fully developed post-chamber downstream pressure.

3.3. Single-orifice plate performance

The single-orifice plate reduced the downstream peak pressure by 51.2 ± 6.1%. This performance is more stable than that of the expansion chamber because the orifice plate imposes a direct geometric restriction on the transmitted wave. The 12 cm diameter opening corresponds to an opening area ratio of 12.6%, forcing the incident shock to interact with a largely closed
plate, reflect upstream, and diffract through the opening. The downstream pressure is therefore reduced by both blockage and wave redistribution. The main design implication is that the plate and its anchorage must resist the local reflected pressure upstream of the orifice.

3.4. Double-orifice plate performance

The double-orifice plate provided the highest reduction among the tested configurations, with an average pressure reduction of 81.9 ± 3.8%. The two plates create sequential restriction stages: the first plate reduces and diffracts the incident wave, and the second plate further attenuates the already disturbed downstream wave. The resulting normalized downstream ratios ranged from 0.14 to 0.24. This two-stage mechanism is therefore more effective than either single-stage restriction or volume enlargement alone.

3.5. Interpretation of experimental and numerical differences

The expansion chamber produced the largest experiment-simulation discrepancy. Physically, this case is more sensitive to local flow expansion, chamber-wall reflection, and the exact sampling location. The downstream sensor is located inside the enlarged chamber region rather than far downstream of a fully developed flow. Consequently, the measured peak pressure may contain reflected and recompressed components that are difficult to reproduce using an idealized geometry. Small assembly tolerances, seams between modular steel components, sensor protrusion, and boundary simplification can therefore strongly influence the local measured peak pressure. For this reason, only the experimental 29.9 ± 9.9% reduction is used for the engineering conclusion.

The single-orifice plate shows the best experiment-simulation consistency because the dominant mechanism is geometric blockage. The effective opening ratio controls the transmitted wave path, and the mean downstream ratio is 0.49 in both the experimental and numerical summaries. This provides a limited validation case for the attenuation-ratio calculation, although it does not replace full pressure-time validation.

The double-orifice plate shows the same qualitative ranking in the experiment and simulation, but the experiment indicates stronger reduction. This may result from three-dimensional detouring, repeated diffraction, local turbulence, and energy loss between the two closely spaced plates. The numerical model may smooth or under-represent some of these localized effects, especially if the mesh and contact definitions simplify the actual plate spacing, edge sharpness, or leakage conditions.

3.6. Design implication of the 12.6% opening ratio

The 12.6% opening ratio should be interpreted as a severe compact-restriction case rather than an optimized value. Literature on barriers and orifice plates indicates that the opening ratio is a dominant factor in shock-wave attenuation because it governs the transmitted area and the strength of upstream reflection. In the present test system, the 12 cm diameter opening provided a practical balance between constructability and strong attenuation. However, because no additional orifice diameters were tested, the results cannot establish an optimal opening ratio. A future design-oriented study should examine larger and smaller opening ratios, plate thickness, edge shape, and spacing between successive plates.

3.7. Practical recommendations

For preliminary protective design, the expansion chamber may be used when space is available and moderate reduction is acceptable. The single-orifice plate is more compact and provides stronger attenuation, but it requires attention to local reflected pressure and anchorage demand. The double-orifice configuration may be considered a promising compact option when downstream peak-pressure reduction is the dominant objective under the tested geometry. This statement is limited to the present 12.6% opening ratio, 7 cm plate spacing, rigid reduced-scale steel model, and P3-P4 measurement definition. It should not be treated as a full-scale design recommendation until plate loads, anchorage demand, structural deformation, alternative opening ratios, alternative spacings, and similarity effects are validated.

3.8. Limitations

The study has five main limitations. First, the tests were conducted using a controlled reducedscale steel model and are not claimed to represent a complete full-scale design standard. Second, only one tunnel cross-section, one orifice diameter, and one double-plate spacing were tested; the 7 cm spacing is a compact modular arrangement and should not be interpreted as an optimized inter-plate distance. Third, the reported standard deviations summarize variation across charge masses and should not be interpreted as shot-to-shot repeatability statistics. Fourth, complete experimental pressure-time histories and impulse values were not uniformly recoverable from the archived compiled dataset. The added waveform figure is therefore adapted from the source thesis numerical pressure-time histories for the single- and double-orifice cases only, and no complete experimental chamber waveform is claimed. Fifth, the numerical observations are used only to support qualitative interpretation and are not used as an independent computational design method.

4. Conclusions

1. The expansion chamber, single-orifice plate, and double-orifice plate reduced downstream peak pressure by $29.9 \pm 9.9\%$, $51.2 \pm 6.1\%$, and $81.9 \pm 3.8\%$, respectively, across the five tested C4 charge masses. The experimental ranking was therefore double-orifice plate > single-orifice plate > expansion chamber.

2. The expansion chamber is useful as a moderate mitigation measure where sufficient space is available, but its performance is sensitive to local reflection and chamber-transition effects. It should not be treated as equivalent to a compact restriction device.

3. The 12.6% single-orifice plate provided stronger and more consistent pressure reduction than the expansion chamber, confirming that geometric blockage and diffraction are effective mechanisms for internal tunnel blast mitigation.

4. The double-orifice plate produced the lowest measured P4/P3 ratio within this bounded test program because it introduced two closely spaced restriction-diffraction stages. It is therefore a promising compact configuration under the tested 12.6% opening ratio and 7 cm plate spacing, but it should not be generalized as a universal design recommendation. The upstream reflected pressure for the orifice-plate configurations may significantly exceed the transmitted downstream pressure; design of plate anchors should account for this amplified local loading.

5. Relative to the straight baseline tunnel, the mean P4/P3 ratio decreased from 0.86 to 0.70, 0.49, and 0.18 for the expansion chamber, single-orifice plate, and double-orifice plate, respectively. The archived pressure-time histories adapted from the source thesis are used only as supplementary qualitative interpretation of waveform shape and arrival sequence. The experimental peak-pressure data form the quantitative basis of the device ranking and define the applicable scope of the findings.

5. Acknowledgements

The authors acknowledge the technical support associated with reduced-scale blast testing, pressure instrumentation, numerical interpretation, and data organization. No external funding is declared in this manuscript.

References

[1] Department of the Army. *TM 5-1300: Structures to Resist the Effects of Accidental Explosions*. U.S. Department of the Army. Washington, DC, 1990.

[2] Department of the Army. *TM 5-855-1: Fundamentals of Protective Design for Conventional Weapons*. U.S. Department of the Army. Washington, DC, 1998.

[3] P. D. Smith, P. Vismeg, L. C. Teo, and L. Tingey, (1998) *"Blast wave transmission along rough-walled tunnels"* **International Journal of Impact Engineering *21***(6): 419–432. DOI: 10.1016/S0734-743X(98)00003-7.

[4] A. Britan, O. Igra, G. Ben-Dor, and H. Shapiro, (2006) *"Shock wave attenuation by grids and orifice plates"* **Shock Waves *16***: 1–15. DOI: 10.1007/s00193-006-0019-0.

[5] G. W. McMahon, J. R. Britt, and B. C. Patterson. "Airblast Propagation within Tunnels from Portal Detonations". In: *Proceedings of the 18th Military Aspects of Blast and Shock*. Bad Reichenhall, Germany, 2004.

[6] G. W. McMahon and S. R. Taylor. *In-Tunnel Airblast from Near-Portal Detonations*. Tech. rep. Vicksburg, MS, USA: Engineer Research and Development Center, 2005.

[7] S. Berger, G. Ben-Dor, and O. Sadot, (2015) *"Experimental and numerical investigations of shock-wave attenuation by geometrical means: A single barrier configuration"* **European Journal of Mechanics - B/Fluids *50***: 60–70. DOI: 10.1016/j.euromechflu.2014.11.006.

[8] S. Berger, G. Ben-Dor, and O. Sadot, (2015) *"Numerical investigation of shock-wave attenuation by geometrical means: Double barrier configuration"* **Journal of Fluids Engineering *137***(4): 041203. DOI: 10.1115/1.4028875.

[9] M. Eslami, P. K. MirzaMohammadi, S. H. Khalilpour, H. Parsa, and V. Kodur, (2023) *"Experimental and numerical investigation of blast wave attenuation by using barriers in different configurations and shapes"* **Journal of Structural Engineering *149***(1): 04022200. DOI: 10.1061/JSENDH.STENG-11408.

[10] P. K. MirzaMohammadi, S. H. Khalilpour, H. Parsa, and P. Sareh, (2023) *"Symmetric multipath branching as a layout design strategy for blast-resilient tunnel structures"* **Structures *58***: 105616. DOI: 10.1016/j.istruc.2023.105616.

[11] O. S. Isaac, O. G. Alshammari, E. G. Pickering, S. D. Clarke, and S. E. Rigby, (2023) *"Blast wave interaction with structures - an overview"* **International Journal of Protective Structures *14***(4): 584–630. DOI: 10.1177/20414196221118595.

[12] C. W. Hung and C. C. Tai, (2021) *"Numerical study of pressure attenuation effect on tunnel explosion"* **Applied Sciences *11***(12): 5646. DOI: 10.3390/app11125646.

[13] Z. Wu, D. Jin, B. Yu, S. Chen, S. Deng, X. Song, W. Yu, Y. Sui, H. Wu, W. Shi, and M. Wang, (2025) *"Experimental and numerical investigation on shock wave attenuation in a chamber"* **Scientific Reports *15***: 11493. DOI: 10.1038/s41598-025-93836-2.

[14] V. Vinod, G. P. Majji, S. V. Anil, R. O. Ram, and L. D. Chandrala, (2025) *"Attenuation of blast waves using rigid porous plate arrays: Insights from experiments and simulations"* **Physics of Fluids *37***(7): 076135. DOI: 10.1063/5.0273908.

[15] V. M. Deshpande and T. Chakraborty, (2024) *"Numerical analysis of a tunnel subjected to blast loads in a transversely isotropic rock mass"* **International Journal of Geomechanics *24***(10): 04024214. DOI: 10.1061/IJGNAI.GMENG-9274.

[16] J. Li, Y. Wang, J. Huang, B. Du, Z. Zong, and M. Li, (2026) *"Blast wave propagation and overpressure prediction in a tunnel with one closed end"* **Tunnelling and Underground Space Technology *170***: 107370. DOI: 10.1016/j.tust.2025.107370.

[17] J. O. Hallquist. *LS-DYNA Theory Manual*. Livermore Software Technology Corporation. Livermore, CA, 2006.

[18] Livermore Software Technology Corporation. *LS-DYNA Keyword User's Manual, Version 971*. Livermore Software Technology Corporation. Livermore, CA, 2012.

[19] Y. H. Bi. *"Numerical Simulation and Validation of Shock Wave Propagation within a Tunnel"*. (mathesis). Taoyuan, Taiwan: National Defense University, 2013.

[20] PCB Piezotronics. *Model 113A23 ICP Pressure Sensor Specification Sheet*. PCB Piezotronics. Depew, NY, 2012.